MOX-Report No. 50/2015

Non-Linear Model for Compression Tests on Articular Cartilage

Grillo, A.; Guaily, A.; Giverso, C.; Federico, S.

MOX, Dipartimento di Matematica
Politecnico di Milano, Via Bonardi 9 - 20133 Milano (Italy)

mox-dmat@polimi.it http://mox.polimi.it

Non-Linear Model for Compression Tests on Articular Cartilage

Alfio Grillo[1], Amr Guaily[2], Chiara Giverso[3], Salvatore Federico[4]

September 28, 2015

[1] Department of Mathematical Sciences (DISMA) – Politecnico di Torino,
Corso Duca degli Abruzzi 24, 10129 Torino, Italy

[2] Engineering Mathematics and Physics Department – Cairo University,
Cairo University Rd, 12613, Giza, Egypt

[3] MOX, Department of Mathematics – Politecnico di Milano,
and Fondazione Centro Europeo Nanomedicina,
Piazza Leonardo da Vinci, 32, 20133 Milano, Italy

[4] Department of Mechanical and Manufacturing Engineering – The University of Calgary,
2500 University Drive NW, Calgary, Alberta, T2N1N4, Canada

Keywords:

Abstract

Hydrated soft tissues, such as articular cartilage, are often modelled as biphasic systems with individually incompressible solid and fluid phases, and biphasic models are employed to fit experimental data in order to determine the mechanical and hydraulic properties of the tissues. Two of the most common experimental setups are confined and unconfined compression. Analytical solutions exist for the unconfined case with the linear, isotropic, homogeneous model of articular cartilage, and for the confined case with the non-linear, isotropic, homogeneous model. The aim of this contribution is to provide an easily implementable numerical tool to determine a solution to the governing differential equations of (homogeneous and isotropic) unconfined and (inhomogeneous and isotropic) confined compression under large deformations. The large-deformation governing equations are reduced to equivalent diffusive equations, which are then solved by means of Finite Difference methods. The solution strategy proposed here could be used to generate benchmark tests for validating complex user-defined material models within Finite Element implementations, and for determining the tissue's mechanical and hydraulic properties from experimental data.

1 Introduction

Since its introduction, the biphasic model of articular cartilage [1–3] has been the standard manner to study also other hydrated soft tissues. In this model, cartilage is represented as the mixture of an incompressible solid, representing structural macromolecules such as collagen fibres and proteoglycans, and an incompressible fluid, representing the interstitial water, along with the various chemical species dissolved in it. In order to fully characterise the behaviour of cartilage according to the biphasic model, it is necessary to experimentally evaluate its elastic properties and its permeability (which is the parameter accounting for the solid-fluid interaction). The most common tests are confined and unconfined compression. In the former, a cartilage sample is placed in an impermeable, rigid chamber and compressed by a porous, rigid piston, so that the fluid can escape from the sample through the piston. In the latter, cartilage is squeezed between two impermeable, rigid plates, so that it can freely expand laterally and fluid can freely escape through the lateral boundary.

Aside from many studies based on Finite Element Analysis, confined and unconfined compression have been also modelled analytically in some particular cases. Based on the linear biphasic model of articular cartilage [1–3], Armstrong et al. [4] derived an analytical solution for the unconfined compression test under small deformations, in terms of series expansions. Holmes and Mow [5] proposed an isotropic homogeneous model of articular cartilage, with non-linear elasticity and deformation-dependent permeability, and studied the case of confined compression analytically. Moreover, in a previous work [6], unconfined compression has been solved numerically under small

deformations for a linear, isotropic, inhomogeneous model. However, these specific cases cannot be used to describe many experimental set-up conditions.

In this work, based on the large-strain governing equations of a biphasic mixture (e.g., [7–9]), we propose a solution to the differential equations of both unconfined and confined compression problems under large deformations, with isotropic non-linear elasticity and deformation-dependent permeability [5]. The case of unconfined compression is studied under the hypothesis of homogeneity, whereas in that of confined compression the elastic properties and permeability are inhomogeneous, as obtained from published experimental works [10, 11], and similarly to what has been done in [6] for the small-deformation case.

Once the hyperelastic constitutive equations are set, the governing equations consist of a system of 4 differential equations in 4 unknowns: three components of the configuration map (treated in terms of their derivatives, i.e., the components of the deformation gradient tensor), and the fluid pressure. For the cases of homogeneous unconfined compression and inhomogeneous confined compression, the material gradient of the pressure is eliminated, yielding a single scalar equation in the volume ratio of the diffusion-advection type, which simplifies remarkably the mathematical problem. The solution that we propose is obtained numerically via a direct application of Finite Difference schemes, and can be used as a rapid, yet effective, comparison solution to verify the robustness and accuracy of complex user-defined material models within Finite Element methods. Furthermore, the proposed implementation is easily manageable and makes the code potentially useful in the determination of mechanical parameters, directly fitting experimental curves.

2 Balance Laws

Here, the description of articular cartilage is limited to the macro-scale, which is interpreted as the laboratory scale at which constitutive information on the overall mechanical behaviour of a given sample of tissue is extracted by means of experiments. At this scale, the tissue is modelled as a biphasic mixture comprising a solid and a fluid phase. The solid phase is the macro-scale representation of a deformable porous medium, which, in fact, is itself a mixture composed mainly of proteoglycans and collagen fibres. The fluid phase represents the interstitial fluid, which occupies the voids of the porous medium and consists mainly of water, ions and various types of chemical compounds, such as nutrients for the cells and byproducts of the cellular metabolism [12].

In the following, the subscripts ‘s’ and ‘f’ shall specify whether a given physical quantity is associated with the solid or with the fluid phase. When there is no danger of confusion, the terms “phase” and “constituent” shall be used interchangeably. The mass distribution of the αth phase of the mixture ($\alpha = \mathrm{f}, \mathrm{s}$), can be expressed either per unit volume occupied by the αth phase itself, or per unit volume of the mixture as a whole. In the first case, one speaks of the “true”, or intrinsic, mass density ρ_α of the αth phase. In the second case, instead, one introduces the “apparent” mass density $\phi_\alpha \rho_\alpha$, with ϕ_α being the volumetric fraction of the αth phase, i.e., the ratio between the size of the

volume occupied by αth phase and the size of a representative volume for the mixture as a whole. Note that the mixture is subjected to the saturation constraint $\phi_{\mathrm{s}} + \phi_{\mathrm{f}} = 1$. All the balance laws referred to the macro-scale description of the mixture's constituents are formulated by employing the apparent mass densities of the phases.

In the absence of sources and sinks of mass, the spatial, local form of the mass balance laws associated with the fluid and the solid phase can be written as

$$\partial_t(\phi_{\,\mathrm{f}}\rho_{\mathrm{f}}) + \mathrm{div}(\phi_{\mathrm{f}}\rho_{\mathrm{f}}\boldsymbol{v}_{\mathrm{s}}) + \mathrm{div}\,(\rho_{\mathrm{f}}\boldsymbol{w}) = 0\,, \tag{1a}$$

$$\partial_t(\phi_{\mathrm{s}}\rho_{\mathrm{s}}) + \mathrm{div}(\phi_{\mathrm{s}}\rho_{\mathrm{s}}\boldsymbol{v}_{\mathrm{s}}) = 0\,, \tag{1b}$$

where $\boldsymbol{v}_{\mathrm{s}}$ and $\boldsymbol{v}_{\mathrm{f}}$ are the velocities of the solid and fluid phase, respectively, and $\boldsymbol{w} = \phi_{\mathrm{f}}(\boldsymbol{v}_{\mathrm{f}} - \boldsymbol{v}_{\mathrm{s}})$ is the filtration velocity. For more details on the kinematics of biphasic mixtures, see, for instance, [13]. From here on, the mass densities ρ_{f} and ρ_{s} are assumed to be given constants, which means that both the fluid and the solid phases are regarded as intrinsically incompressible materials. By definition, this means that the substantial derivatives $D_\alpha\rho_\alpha := \partial_t\rho_\alpha + (\mathrm{grad}\rho_\alpha)\boldsymbol{v}_\alpha$ are zero for $\alpha = \mathrm{f}, \mathrm{s}$.

Under the assumption of negligible inertial effects, in the absence of body forces external to the considered mixture, and accepting the validity of Darcy's law, the spatial, local balance laws of momentum associated with the mixture as a whole and the fluid phase can be written as

$$\boldsymbol{0} = \mathrm{div}(\boldsymbol{\sigma}_{\mathrm{f}} + \boldsymbol{\sigma}_{\mathrm{s}})\,, \tag{2}$$

$$\boldsymbol{w} = -\boldsymbol{k}\,\mathrm{grad}\,p\,, \tag{3}$$

where $\boldsymbol{\sigma}_{\mathrm{f}}$ and $\boldsymbol{\sigma}_{\mathrm{s}}$ are the Cauchy stress tensors of the fluid and solid phase, respectively, and $\boldsymbol{k}$ is the spatial permeability tensor. The mixture is assumed to be closed with respect to momentum.

If the fluid phase is modelled as an incompressible and macroscopically inviscid Stokes fluid, the stress tensors for the fluid, the solid and the whole tissue admit the expressions

$$\boldsymbol{\sigma}_{\mathrm{f}} = -\phi_{\mathrm{f}}\,p\,\boldsymbol{g}^{-1}\,, \tag{4a}$$

$$\boldsymbol{\sigma}_{\mathrm{s}} = -\phi_{\mathrm{s}}\,p\,\boldsymbol{g}^{-1} + \boldsymbol{\sigma}_{\mathrm{c}}\,, \tag{4b}$$

$$\boldsymbol{\sigma} = \boldsymbol{\sigma}_{\mathrm{f}} + \boldsymbol{\sigma}_{\mathrm{s}} = -p\,\boldsymbol{g}^{-1} + \boldsymbol{\sigma}_{\mathrm{c}}\,, \tag{4c}$$

where $\boldsymbol{\sigma}_{\mathrm{c}}$ is referred to as the *constitutive part* of $\boldsymbol{\sigma}_{\mathrm{s}}$, p is the hydrostatic pressure, and $\boldsymbol{g}^{-1}$, with components g^{ab}, is the inverse of the spatial metric tensor $\boldsymbol{g}$ and serves here as the "contravariant" identity tensor.

The deformation of the solid phase is denoted by χ, the deformation gradient by $\boldsymbol{F}$ (with components $F^a{}_A = \chi^a{}_{,A}$), and the volume ratio by $J = \det\boldsymbol{F}$. By performing a backward Piola Transformation of (1a) and (1b), which is done by multiplying both equations by J, one obtains

$$\dot{\phi}_{\mathrm{fR}} + \mathrm{Div}(\boldsymbol{W}) = 0\,, \tag{5a}$$

$$\dot{\phi}_{\mathrm{sR}} = 0\,. \tag{5b}$$

In (5a) and (5b), the superimposed dot stands for time differentiation, Div is the material divergence operator, and

$$\phi_{\mathrm{sR}} = J\phi_{\mathrm{s}}\,, \tag{6a}$$

$$\phi_{\mathrm{fR}} = J\phi_{\mathrm{f}} = J - \phi_{\mathrm{sR}}\,, \tag{6b}$$

$$\boldsymbol{W} = J\boldsymbol{F}^{-1}\boldsymbol{w} = -\boldsymbol{K}\,\mathrm{Grad}\,p\,, \tag{6c}$$

with $\boldsymbol{K} = J\boldsymbol{F}^{-1}\boldsymbol{k}\,\boldsymbol{F}^{-\mathrm{T}}$ being the material permeability tensor, are the Piola transforms of ϕ_{f}, ϕ_{s} and $\boldsymbol{w}$. In particular, (6a) can be used to express ϕ_{s} as a function of the volume ratio of the solid phase, i.e., $\phi_{\mathrm{s}} = J^{-1}\phi_{\mathrm{sR}}$. This result, which stems from the incompressibility of the solid phase, permits to rephrase the inequalities $0 \leq \phi_{\mathrm{s}}(x,t) \leq 1$ (with the upper bound condition $\phi_{\mathrm{s}}(x,t) = 1$ implying that the limit of *compaction* is reached) as $0 \leq \phi_{\mathrm{sR}}(X) \leq J(X,t)$, and thus it places on J the *unilateral* constraint $J(X,t) \geq \phi_{\mathrm{sR}}(X)$ [8]. In particular, when the condition $J = \phi_{\mathrm{sR}}$ is met at a given point X of the reference configuration $\mathcal{B}_{\mathrm{R}}$, all fluid has been expelled from the point, which thereby remains composed of solid alone, which is incompressible by hypothesis. It is worth to recall that, for a biphasic mixture, the requirement that both phases are intrinsically incompressible, does *not* lead to the restriction $J = 1$ of isochoric motion, due to the presence of the volumetric fraction ϕ_{s} in (1b). Indeed, the assumption of incompressibility, which is translated into $D_{\mathrm{s}}\rho_{\mathrm{s}} = 0$, transforms (1b) into an equation for ϕ_{s}, whose variations are compensated for by the change of volume of the solid phase. In the material formalism, this fact is reflected by (6a), which allows to express ϕ_{s} as a function of J. An extensive discussion about this issue and, in particular, on the consequences of compaction, is given in [8].

Finally, by adding together (5a) and (5b), using (6c), and performing a Piola transformation of (2), with $\boldsymbol{\sigma}_{\mathrm{f}}$ and $\boldsymbol{\sigma}_{\mathrm{s}}$ given by (4b) and (4a), the material form of the mass and momentum balance laws becomes

$$\dot{J} = \mathrm{Div}\,(\boldsymbol{K}\,\mathrm{Grad}\,p)\,, \tag{7a}$$

$$\mathrm{Div}\,\boldsymbol{P}_{\mathrm{c}} = J\,\boldsymbol{g}^{-1}\boldsymbol{F}^{-\mathrm{T}}\mathrm{Grad}\,p\,, \tag{7b}$$

where $\boldsymbol{P}_{\mathrm{c}} = J\,\boldsymbol{\sigma}_{\mathrm{c}}\,\boldsymbol{F}^{-\mathrm{T}}$ is the constitutive part of the first Piola-Kirchhoff stress tensor of the solid phase. Furthermore, the first Piola-Kirchhoff stress for the whole tissue is obtained by Piola-transforming (4c), which yields $\boldsymbol{P} = -J\,p\,\boldsymbol{g}^{-1}\boldsymbol{F}^{-\mathrm{T}} + \boldsymbol{P}_{\mathrm{c}}$.

3 Constitutive Laws and Final Model Equations

The non-linear isotropic model proposed by Holmes and Mow [5] is adopted in this work. The solid phase is regarded as hyperelastic, with potential

$$\hat{W}(\boldsymbol{C}) = \alpha_0\,(\exp[\varphi(\boldsymbol{C})] - 1)\,, \tag{8a}$$

$$\varphi(\boldsymbol{C}) = \alpha_1\big[I_1(\boldsymbol{C}) - 3\big] + \alpha_2\big[I_2(\boldsymbol{C}) - 3\big] - \beta\ln\left[I_3(\boldsymbol{C})\right], \tag{8b}$$

where $\alpha_0, \alpha_1, \alpha_2$, and β are material parameters, and $I_1(\boldsymbol{C}) = \mathrm{tr}(\boldsymbol{C})$, $I_2(\boldsymbol{C}) = \frac{1}{2}[(\mathrm{tr}(\boldsymbol{C}))^2 - \mathrm{tr}(\boldsymbol{C}^2)]$, and $I_3(\boldsymbol{C}) = \det(\boldsymbol{C})$ are the invariants of the right Cauchy-Green deformation tensor $\boldsymbol{C} = \boldsymbol{F}^{\mathrm{T}}.\boldsymbol{F}$. Thus, $\boldsymbol{P}_{\mathrm{c}}$ is given by

$$\boldsymbol{P}_{\mathrm{c}} = \hat{\boldsymbol{P}}_{\mathrm{c}}(\boldsymbol{F}) = \boldsymbol{F}\left(2\frac{\partial \hat{W}}{\partial \boldsymbol{C}}(\boldsymbol{C})\right). \tag{9}$$

The permeability is assumed to be related to J via the Holmes-Mow law [5]

$$k = \hat{k}(J) = k_0\left(\frac{J-\phi_{\mathrm{sR}}}{1-\phi_{\mathrm{sR}}}\right)^{\gamma}\exp\left(\tfrac{M}{2}(J^2-1)\right), \tag{10}$$

where γ and M are material parameters, $\hat{k}(J) = k$ denotes the constitutive function associated with the scalar permeability k, and $k_0 = \hat{k}(1)$ is the value of the permeability in the undeformed configuration ($J = 1$). In order to satisfy (7a), $\hat{k}$ must vanish at compaction, i.e., at $J = \phi_{\mathrm{sR}}$, so that $\dot{J}$ vanishes too, and the incompressibility constraint is respected. As an isotropic tensor-valued function, the permeability is assumed to be spherical [14], so that the spatial and material permeability tensors are given by

$$\boldsymbol{k} = k\,\boldsymbol{g}^{-1} = \hat{k}(J)\,\boldsymbol{g}^{-1}, \tag{11a}$$

$$\boldsymbol{K} = \hat{\boldsymbol{K}}(\boldsymbol{C}) = J\,\hat{k}(J)\,\boldsymbol{C}^{-1}. \tag{11b}$$

In (10), $\hat{k}$ vanishes for $J = \phi_{\mathrm{sR}}$, and therefore $\boldsymbol{k}$ vanishes too. For an inhomogeneous material, $\hat{W}$ and $\hat{\boldsymbol{K}}$ depend explicitly on the material point X, through the parameters $\alpha_0, \alpha_1, \alpha_2, \beta$ and k_0, γ, M, and possibly through ϕ_{sR} as well. Hereafter, cartilage is regarded as homogeneous for the case of unconfined compression and as inhomogeneous for the case of confined compression.

Equations (7a) and (7b) are suitable for computations based on the Finite Element Method (FEM), cf., e.g., [12]. Here, however, a different approach is followed, since the aim of this work is to provide a valid alternative to Finite Element implementations for the considered problems. The reason for undertaking this task is to supply fast estimates about the hydraulic and mechanical properties of cartilage (in the limit case of isotropy), that can be used as reference for testing the reliability of complex, FEM-based numerical strategies, which might be necessary for highly non-linear, coupled, anisotropic and inhomogeneous problems. The first step is the decoupling of (7a) from (7b), which is achieved by substituting $\mathrm{Grad}\,p$, obtained from (7b), into (7a). By accounting for (11b), this yields

$$\dot{J} = \mathrm{Div}\left[\hat{k}(J)\boldsymbol{F}^{-1}\mathrm{Div}\Big(\hat{\boldsymbol{P}}_{\mathrm{c}}(\boldsymbol{F})\Big)\right], \tag{12a}$$

$$\mathrm{Grad}\,p = J^{-1}\boldsymbol{F}^{\mathrm{T}}\boldsymbol{g}\,\mathrm{Div}\Big(\hat{\boldsymbol{P}}_{\mathrm{c}}(\boldsymbol{F})\Big). \tag{12b}$$

Equations (12a) and (12b) have some relevant differences with respect to the original Equations (7a) and (7b). Firstly, p can be computed *a posteriori* by solving (12b),

once (12a) is solved for χ. Secondly, (12b) involves only the first-order space derivatives of p, whereas the Poisson-like equation (7a) also involves the second-order space derivatives of p. Finally, the permeability does not directly affect the pressure. Rather, it influences the solution of (12a), which involves the third-order space derivatives of χ as well as its mixed derivatives (i.e., with respect to both time and space), as prescribed by the computation of $\dot{J}$.

4 Axisymmetric Unconfined Compression

The subject of this section is the study of the unconfined compression test of a cylindrical specimen of cartilage. In this test, the specimen is assumed to be homogeneous and isotropic. Therefore, its permeability and hyperelastic potential are independent of material points, and related to deformation only through the invariants of $\boldsymbol{C}$. Moreover, ϕ_{sR} is a model constant.

The cylindrical specimen is inserted between two rigid and impermeable plates that remain parallel to each other for the whole duration of the experiment. The lower plate is kept fixed, while the upper one moves downward according to a prescribed loading protocol. In this work, only a displacement-control test is considered. The lateral wall of the specimen is traction-free and permeable. The lower and upper surfaces of the specimen are allowed to glide on the lower and upper plate, respectively, in an axisymmetric way. Moreover, no friction is considered, so that the specimen preserves its original cylindrical shape throughout the experiment.

The geometry of the specimen, its material symmetries (homogeneity and isotropy) and the experimental protocol make it convenient to employ cylindrical coordinates $\{R, \Theta, Z\}$ and $\{r, \theta, z\}$ for both the reference (undeformed) and deformed configuration, respectively. Below, the boundary conditions for χ and p, which have to hold at all times, are specified for all portions of the boundary.
At the lower boundary, $(R, \Theta, Z) \in [0, R_{\mathrm{ext}}] \times [0, 2\pi[\times \{0\}$,

$$\chi^z = 0\,, \qquad \text{[no displacement]} \tag{13a}$$

$$(-\boldsymbol{K}\mathrm{Grad}\, p)\,.(-\boldsymbol{E}_Z) = 0\,, \qquad \text{[no flux]} \tag{13b}$$

where χ^z is the axial component of the deformation χ, and $\boldsymbol{E}_Z$ is the unit vector pointing upward and aligned along the axial direction.
At the upper boundary, $(R, \Theta, Z) \in [0, R_{\mathrm{ext}}] \times [0, 2\pi[\times \{H\}$,

$$\chi^z = \lambda_Z H\,, \tag{14a}$$

$$\lambda_Z(t) = 1 - \frac{u_T}{H}\left[1 - \exp(-t/t_u)\right]\,, \qquad \text{[prescribed stretch]} \tag{14b}$$

$$(-\boldsymbol{K}\mathrm{Grad}\, p)\,.\,\boldsymbol{E}_Z = 0\,, \qquad \text{[no flux]} \tag{14c}$$

where H is the initial height of the specimen, and λ_Z is the imposed time-dependent stretch, with target displacement u_T and time constant t_u.

At the lateral boundary, $(R, \Theta, Z) \in \{R_{\text{ext}}\} \times [0, 2\pi[\,\times[0, H]$,

$$-\,p = 0\,, \qquad \text{[atmospheric pressure]} \tag{15a}$$

$$\boldsymbol{P}.\boldsymbol{E}_R = \boldsymbol{0}\,, \qquad \text{[traction-free boundary]} \tag{15b}$$

where $\boldsymbol{E}_R$ is the referential radial unit vector, pointing outward and aligned along the radial direction. Finally, the axial symmetry of the problem places the further restriction that the radial deformation and the radial fluid flux must vanish at the origin of each cross section of the specimen. Since the reference configuration is assumed to coincide with the stress-free, undeformed one, the initial conditions $p(X, 0) = 0$ and $\chi(X, 0) = X$ apply at all inner points X of the computational domain.

It should be remarked that (15b) involves the overall first Piola-Kirchhoff stress tensor of the mixture as a whole. Since it holds that $\boldsymbol{P} = -J\,p\,\boldsymbol{g}^{-1}\boldsymbol{F}^{-\mathrm{T}} + \boldsymbol{P}_{\mathrm{c}}$, and pressure has to vanish on the lateral boundary of the specimen, (15b) can also be rephrased in terms of the constitutive part of $\boldsymbol{P}$, i.e. $\boldsymbol{P}_{\mathrm{c}}.\boldsymbol{E}_R = \boldsymbol{0}$.

4.1 Specific Form of the Deformation

Due to the symmetries of the problem, χ acquires the form

$$r = \chi^r(R, \Theta, Z, t) \equiv f(R, t)\,, \tag{16a}$$

$$\vartheta = \chi^\vartheta(R, \Theta, Z, t) = \Theta\,, \tag{16b}$$

$$z = \chi^z(R, \Theta, Z, t) = \lambda_Z(t)\,Z\,. \tag{16c}$$

In (16a), χ^r is re-defined as a function f of R and t alone, and $\lambda_Z(t)$ is the uniform axial stretch, as defined in (14b). The latter is a function known from the boundary conditions on the displacement in the axial direction for the case of a displacement-controlled test. The stretches in the radial and circumferential direction are given by

$$\lambda_R(R, t) = \frac{\partial f}{\partial R}(R, t) \equiv f'(R, t), \tag{17a}$$

$$\lambda_\Theta(R, t) = \frac{f(R, t)}{R}. \tag{17b}$$

Thus, the matrix representation of $\boldsymbol{F}$, which is diagonal, and the volume ratio J become

$$[F^a{}_A](R, t) = \mathrm{diag}[\lambda_R(R, t), \lambda_\Theta(R, t), \lambda_Z(t)]\,, \tag{18a}$$

$$J(R, t) = f'(R, t)\,\frac{f(R, t)}{R}\,\lambda_Z(t)\,. \tag{18b}$$

4.2 Stress and Balance Equations

Because of the deformation specified by (16a)–(16c), the matrix representation of $\boldsymbol{P}_{\mathrm{c}}$ is diagonal. Moreover, the equation of the balance of mass (12a), and the only non-

trivially satisfied component of the equation of balance of momentum (12b) read

$$\dot{J} = \left(\frac{\partial}{\partial R} + \frac{1}{R}\right)\left[\frac{\hat{k}(J)}{\lambda_R}\left(\frac{\partial P_{\mathrm{c}}^{rR}}{\partial R} + \frac{P_{\mathrm{c}}^{rR} - P_{\mathrm{c}}^{\vartheta\Theta}}{R}\right)\right], \tag{19a}$$

$$\frac{\partial p}{\partial R} = \frac{\lambda_R}{J}\left(\frac{\partial P_{\mathrm{c}}^{rR}}{\partial R} + \frac{P_{\mathrm{c}}^{rR} - P_{\mathrm{c}}^{\vartheta\Theta}}{R}\right). \tag{19b}$$

Since P_{c}^{rR} and $P_{\mathrm{c}}^{\vartheta\Theta}$ are constitutive functions of λ_R, λ_Θ and λ_Z, and since λ_R and λ_Θ involve the radial deformation f, while λ_Z is known from the outset, the right-hand-side of (19a) can be recast as a combination of terms in the unknown f and its radial derivatives up the third-order. Thus, after substituting the constitutive laws, an equation for f can be obtained.

Since (19b) is decoupled from (19a), it suffices to determine f by solving (19a) and then compute p through (19b).

4.3 "Diffusive Equation"

Solving (19a) may be cumbersome, since it is a highly non-linear partial differential equation of the third-order in the radial derivatives of f, and it involves the mixed derivatives of f with respect to time and the radial coordinate. The scope of this section is to show that (19a) can be transformed into a pseudo-diffusion-reaction equation in J. To achieve this goal, the first step consists of the change of variables

$$f'(R,t) = \lambda_R(R,t) = \frac{R\,J(R,t)}{f(R,t)\lambda_Z(t)}. \tag{20}$$

Accordingly, λ_R can be viewed as a function of J, f, λ_Z and R, where the dependence on $\lambda_Z(t)$, which is known from the outset, can be rephrased as an explicit dependence on time. Similarly, λ_Θ can be regarded as a function of f and R. Hence, the stresses P_{c}^{rR} and $P_{\mathrm{c}}^{\vartheta\Theta}$ can be reformulated as follows:

$$P_{\mathrm{c}}^{rR} = \tilde{P}_{\mathrm{c}}^{rR}(J(R,t), f(R,t), \lambda_Z(t), R), \tag{21a}$$

$$P_{\mathrm{c}}^{\vartheta\Theta} = \tilde{P}_{\mathrm{c}}^{\vartheta\Theta}(J(R,t), f(R,t), \lambda_Z(t), R). \tag{21b}$$

By substituting the right-hand-sides of (21a) and (21b) into (19a), and performing some algebraic manipulations that account for the new definitions of stress (21a) and (21b), it is possible to define the quantities

$$\mathcal{D} := \frac{k}{\lambda_R}\frac{\partial \tilde{P}_{\mathrm{c}}^{rR}}{\partial J}, \tag{22a}$$

$$-\mathcal{A}J := \frac{k}{\lambda_R}\left\{\frac{\partial \tilde{P}_{\mathrm{c}}^{rR}}{\partial f}\lambda_R + \left.\frac{\partial \tilde{P}_{\mathrm{c}}^{rR}}{\partial R}\right|_{\mathrm{exp}} + \frac{\tilde{P}_{\mathrm{c}}^{rR} - \tilde{P}_{\mathrm{c}}^{\vartheta\Theta}}{R}\right\}, \tag{22b}$$

where $\left[\partial(\,\cdot\,)/\partial R\right]\big|_{\mathrm{exp}}$ represents the explicit derivative along the radial direction. Consequently, (19a) takes the form of a diffusion-advection equation in the variable J (the

transported field), i.e.,

$$\dot{J} = \left(\frac{\partial}{\partial R} + \frac{1}{R}\right)\left[\mathcal{D}\frac{\partial J}{\partial R} - \mathcal{A}J\right], \tag{23}$$

with $\mathcal{D}$ and $\mathcal{A}$ playing the role of the diffusion coefficient and advection velocity, respectively. The physical units of $\mathcal{D}$ and $\mathcal{A}$, which are given by $[\mathcal{D}] = \mathrm{length}^2/\mathrm{time}$ and $[\mathcal{A}] = \mathrm{length}/\mathrm{time}$, show that these identifications are physically sound.

It is worth to mention that $\mathcal{D}$ stems from the combination of very important physical entities. These are the permeability, which encapsulates all information about the hydraulic response of the system, and the derivative of $\tilde{P}_{\mathrm{c}}^{rR}$ with respect to J, which is related to the acoustic tensor of the solid phase. Analogous considerations hold true for the drift velocity $\mathcal{A}$. In this case, however, also the term $(\tilde{P}_{\mathrm{c}}^{rR} - \tilde{P}_{\mathrm{c}}^{\vartheta\Theta})/R$ contributes to advection.

The coefficients $\mathcal{D}$ and $\mathcal{A}$ can be expressed as functions of J, f, λ_Z and R. Therefore, the diffusion-advection equation (23) is coupled with the radial deformation f, which can be determined by solving (20). In conclusion, the change of variables (20) rephrases the mathematical structure of (19a) and (19b) into the following set of new model equations:

$$f'(R,t) = \frac{RJ(R,t)}{f(R,t)\lambda_Z(t)}, \tag{24a}$$

$$\dot{J} = \frac{1}{R}\frac{\partial}{\partial R}\left\{R\left[\mathcal{D}\frac{\partial J}{\partial R} - \mathcal{A}J\right]\right\}, \tag{24b}$$

$$\frac{J}{\lambda_R}\frac{\partial p}{\partial R} = \frac{\lambda_R}{\hat{k}(J)}\left[\mathcal{D}\frac{\partial J}{\partial R} - \mathcal{A}J\right]. \tag{24c}$$

This set consists of three independent scalar equations in the three unknowns J, f and p. Clearly, the boundary conditions must be rewritten accordingly:

$$f(0,t) = 0 \qquad [\text{axial symmetry}], \tag{25a}$$

$$\left(\mathcal{D}\frac{\partial J}{\partial R} - \mathcal{A}J\right)\Big|_{R=0} = 0 \qquad [\text{axial symmetry}], \tag{25b}$$

$$p(R_{\mathrm{ext}},t) = 0 \qquad [\text{from (15a)}], \tag{25c}$$

$$\tilde{P}_{\mathrm{c}}^{rR}(J,f,\lambda_Z(t),R)\Big|_{R=R_{\mathrm{ext}}} = 0 \qquad [\text{from (15b)}]. \tag{25d}$$

Note that (25a) is a homogeneous Dirichlet condition on f (only one boundary condition is needed for f, since (24a) is of the first order), (25b) and (25d) express, respectively, a homogeneous Robin condition and a Dirichlet condition on J, while (25c) is a Dirichlet condition on p. Finally, the initial conditions read $f(R,0) = R$, $J(R,0) = 1$, and $p(R,0) = 0$, for all $R \in [0, R_{\mathrm{ext}}]$.

4.4 Discretisation and Results

Let $[0,T]$ be the interval of time over which the system is observed, and let $0 = t_0 < t_1 < \ldots < t_N = T$ be a partition of $[0,T]$, where $\tau_n = t_n - t_{n-1}$ is the amplitude of

the subinterval $[t_{n-1}, t_n] \subset [0, T]$, for $n = 1, \ldots, N$, and N is the total number of such sub-intervals. Similarly, $[0, R_{\text{ext}}]$ is partitioned as $0 = R_0 < R_1 < \ldots < R_M = R_{\text{ext}}$, with $\Delta_m = R_m - R_{m-1}$ being the amplitude of $[R_{m-1}, R_m] \subset [0, R_{\text{ext}}]$, for $m = 1, \ldots, M$. Given a generic function q of the radial coordinate and time, the notation $q_{m,n} = q(R_m, t_n)$ indicates that q is evaluated at the point (R_m, t_n) of the space-time grid constructed above.

Due to the high non-linearity of the system, especially in $\mathcal{D}$ and $\mathcal{A}$, an explicit Euler method in time is chosen for (24b). To avoid the occurrence of numerical instabilities, the amplitudes Δ_m and τ_n, which measure, respectively, the increments in space and time, are required to satisfy the constraint $\Delta_m^2/2\tau_n \leq \mathcal{D}_{\text{ref}}$, for all $m = 1, \ldots, M$, and for all $n = 1, \ldots, N$, where $\mathcal{D}_{\text{ref}}$ is a constant, referential value of the diffusion coefficient.

The discretised form of (24a)–(24c) is given by

$$f_{m,n} - f_{m-1,n} = \Delta_m \frac{R_m J_{m,n}}{f_{m,n} \lambda_Z(t_n)}, \tag{26a}$$

$$J_{m,n} - J_{m,n-1} = \tau_n \left[\frac{Q_{m,n-1} - Q_{m-1,n-1}}{\Delta_m} + \frac{Q_{m,n-1}}{R_m} \right], \tag{26b}$$

$$\frac{p_{m,n} - p_{m-1,n}}{\Delta_m} = \frac{(\lambda_{Rm,n})^2}{J_{m,n} k_{m,n}} Q_{m,n}\,, \tag{26c}$$

with $m = 1, \ldots, M$ and $n = 1, \ldots, N$. For all $p = 0, \ldots, M-1$, and for all $q = 0, \ldots, N$, Q_{pq} is defined as

$$Q_{p,q} = \mathcal{D}_{p,q} \frac{J_{p+1,q} - J_{p,q}}{\Delta_p} - \mathcal{A}_{p,q} J_{p,q}\,. \tag{27}$$

The equations have been implemented independently both in Fortran and in Matlab©.

For the simulation of the homogeneous unconfined compression, the parameters specifying the Holmes-Mow permeability defined in (10) are given by $k_0 = 2.519 \cdot 10^{-3}\ \text{mm}^2\,\text{MPa}^{-1}\,\text{s}^{-1}$, $M = 4.638$, $\gamma = 0.0848$, and $\phi_{\text{sR}} = 0.2$, while the constants that characterise the Holmes-Mow hyperelastic potential (8) are taken as $\alpha_0 = 0.11$ MPa, $\alpha_1 = 0.26$, $\alpha_2 = 0.25$, and $\beta = 0.76$. With the exception of α_1 and α_2, whose values were assumed, all these data were taken from the experiments on bovine cartilage reported in [5]. The specimen is a cylinder of height $H = 2$ mm and radius $R_{\text{ext}} = 3$ mm. Finally, the parameters defining the imposed axial stretch are the target axial displacement $u_T = 0.4$ mm (corresponding to a final 20% nominal strain) and the time constant $t_u = 10$ s.

For the whole duration of the simulated experiment, and for the considered set of parameters, only relatively small variations of the volume ratio J (less than the 10%) are observed. Moreover, through most of the (normalised) radius, J remains practically uniform and equal to the initial (undeformed) value of 1, while, close to the lateral boundary, the fluid exudation causes a loss of fluid volume, which is reflected in a decrease in J (Fig. 1). Also the radial component P_{c}^{rR} of the constitutive part of the first Piola-Kirchhoff stress tensor (normalised to the material parameter α_0) remains

virtually uniform through most of the range of the (normalised) radial coordinate, and then decreases to zero to satisfy the boundary condition of zero traction. As time goes on, the stress relaxes because of the exudation of the fluid (Fig. 2).

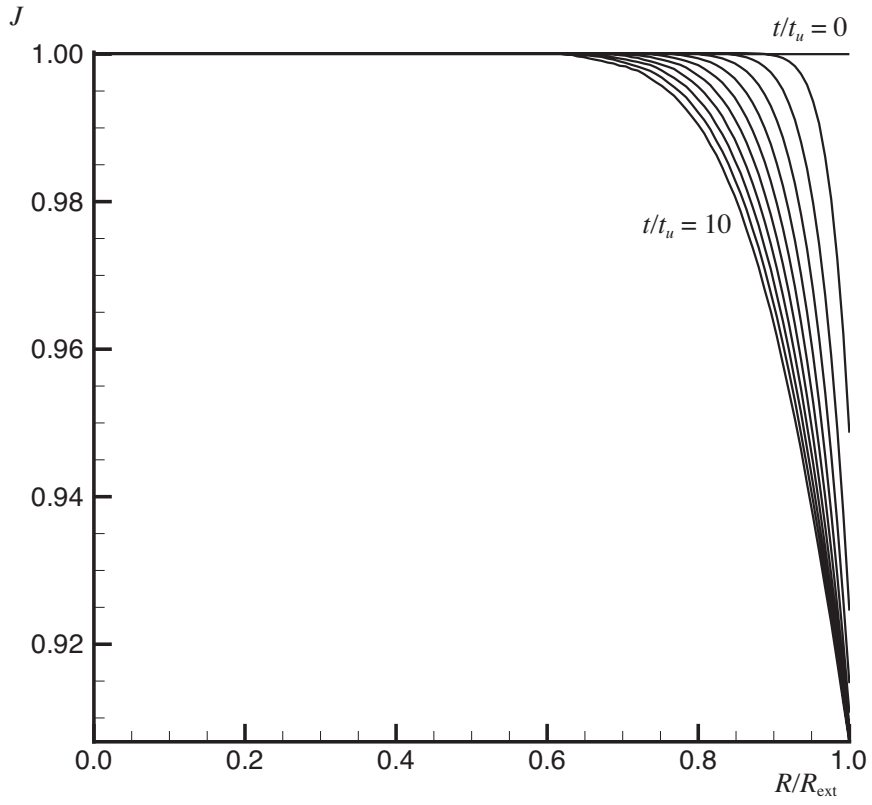

Figure 1: Volume ratio J vs the normalised radial coordinate R/R_{ext}. The curves are plotted for values of the normalised time $t/t_u = 0, 1, ..., 10$.

5 Axisymmetric Confined Compression

This section focuses on another experimental test that is largely used for characterising the hydraulic and mechanical behaviour of articular cartilage: the axisymmetric confined compression test. A specimen of tissue is inserted into a cylindrical, impermeable, rigid chamber and compressed by a porous, rigid piston, so that the fluid can escape through it when the specimen is compressed. In the following, confined compression is simulated in displacement control.

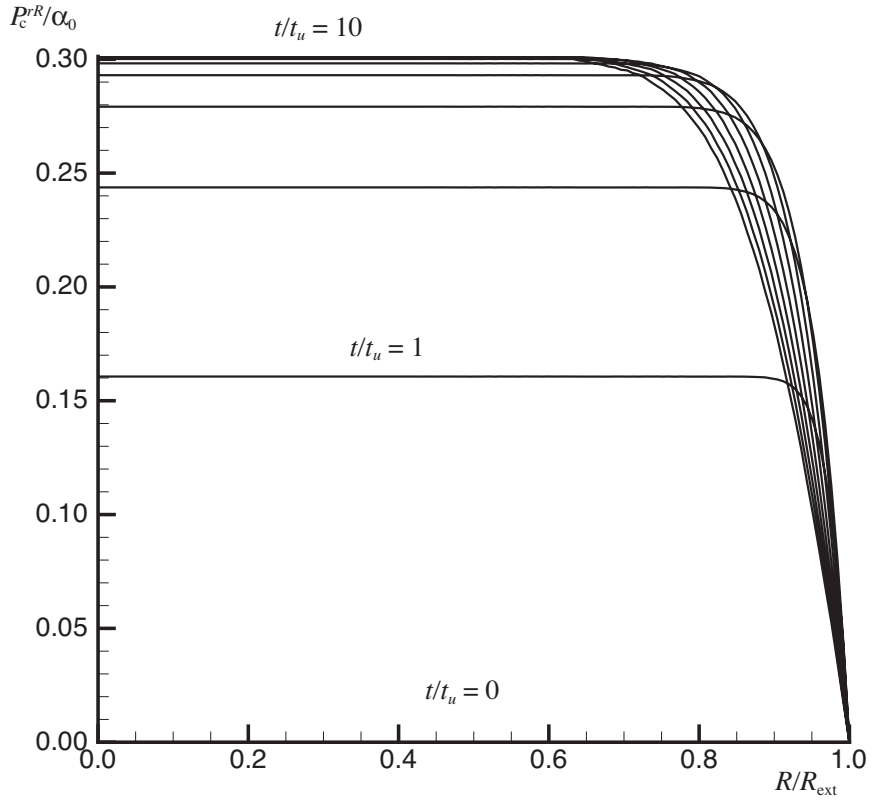

Figure 2: Radial component P_{c}^{rR} of the constitutive part of the first Piola-Kirchhoff stress tensor of the solid phase, normalised to the material parameter α_0, vs the normalised radial coordinate R/R_{ext}. The curves are plotted for values of the normalised time $t/t_u = 0, 1, ..., 10$.

5.1 Specific Form of the Deformation

The solid phase of the tested biphasic medium is isotropic and "transversely homogeneous", i.e., its material properties are allowed to vary only along the axial direction. Furthermore, due to the impermeability of the lower plate and the lateral wall of the chamber, the only non-vanishing component of the fluid velocity is along the symmetry axis of the specimen. In the usual material and spatial cylindrical coordinates $\{R, \Theta, Z\}$ and $\{r, \theta, z\}$, the deformation is given by

$$r = \chi^r(R, \Theta, Z, t) = R\,, \tag{28a}$$

$$\vartheta = \chi^\vartheta(R, \Theta, Z, t) = \Theta\,, \tag{28b}$$

$$z = \chi^z(R, \Theta, Z, t) \equiv \mathfrak{g}(Z, t)\,, \tag{28c}$$

where χ^z has been redefined as a function $\mathfrak{g}$ of the axial coordinate Z and time alone. The matrix representing $\boldsymbol{F}$ (from which that of $\boldsymbol{C}^{-1}$ can be obtained) is

$$[F_A^a](Z,t) = \mathrm{diag}[1, 1, \lambda_Z(Z,t)]\,, \tag{29}$$

since the radial and axial stretches are $\lambda_R = \lambda_\Theta = 1$, while the axial stretch λ_Z satisfies $J = \lambda_Z = \mathfrak{g}'$, at all points and all times, with the prime denoting partial differentiation with respect to the axial coordinate Z.

5.2 Stress and Balance Equations

The form of the deformation specified in (28a)–(28c) implies that also the matrix representing $\boldsymbol{P}_\mathrm{c}$ is diagonal, and its components can be written as

$$P_\mathrm{c}^{rR}(Z,t) = \tilde{P}_\mathrm{c}^{rR}(J(Z,t), Z)\,, \tag{30a}$$
$$P_\mathrm{c}^{\vartheta\Theta}(Z,t) = \tilde{P}_\mathrm{c}^{\vartheta\Theta}(J(Z,t), Z)\,, \tag{30b}$$
$$P_\mathrm{c}^{zZ}(Z,t) = \tilde{P}_\mathrm{c}^{zZ}(J(Z,t), Z)\,, \tag{30c}$$

where the explicit dependence of the constitutive laws on Z has been indicated. Moreover, since all derivatives in directions other than the axial one vanish identically, and since P_c^{rR} and $P_\mathrm{c}^{\vartheta\Theta}$ are equal to each other, the model equations (12a) and (12b) simplify to

$$\dot{J} = \frac{\partial}{\partial Z}\left[\frac{k}{J}\frac{\partial P_\mathrm{c}^{zZ}}{\partial Z}\right]\,, \tag{31a}$$
$$\frac{\partial p}{\partial Z} = \frac{\partial P_\mathrm{c}^{zZ}}{\partial Z}\,, \tag{31b}$$

where the permeability k is now assumed to depend explicitly on the axial coordinate. In this formulation, the unknowns are the axial deformation $\mathfrak{g}$ and the pressure p. If the experiment is performed in displacement control, the following set of boundary and initial conditions must be respected by the unknowns.
At the lower boundary (rigid, at rest, and impermeable),

$$\mathfrak{g}(0,t) = 0\,, \tag{32a}$$
$$\left(\frac{\partial p}{\partial Z}(0,t) = 0 \quad \Rightarrow\right) \frac{\partial P_\mathrm{c}^{zZ}}{\partial Z}(0,t) = 0\,. \tag{32b}$$

At the upper boundary (rigid, moving downward, permeable),

$$\mathfrak{g}(H,t) = H - u_T\left[1 - \exp(-t/t_u)\right]\,, \tag{33a}$$
$$p(H,t) = 0\,. \tag{33b}$$

Furthermore, the initial conditions are given by $\mathfrak{g}(Z,0) = Z$ and $p(Z,0) = 0$, for all $Z \in [0,H]$.

5.3 "Diffusive Equation"

As done in Section 4.3 for the case of the unconfined compression test, (31a) can be reformulated in the form of a pseudo-diffusion-advection equation for the volume ratio J. Indeed, the constitutive definition of P_{c}^{zZ} leads to the relation

$$\frac{\partial P_{\mathrm{c}}^{zZ}}{\partial Z} = \frac{\partial \tilde{P}_{\mathrm{c}}^{zZ}}{\partial J}\frac{\partial J}{\partial Z} + \left.\frac{\partial \tilde{P}_{\mathrm{c}}^{zZ}}{\partial Z}\right|_{\mathrm{exp}}, \tag{34}$$

where the second term on the right-hand-side of (34) denotes the explicit derivative of $\tilde{P}_{\mathrm{c}}^{zZ}$ with respect to the axial coordinate. Thus, by introducing the notation

$$\mathcal{D} := \frac{k}{J}\frac{\partial \tilde{P}_{\mathrm{c}}^{zZ}}{\partial J}, \tag{35a}$$

$$-\mathcal{A}J := \frac{k}{J}\left.\frac{\partial \tilde{P}_{\mathrm{c}}^{zZ}}{\partial Z}\right|_{\mathrm{exp}}, \tag{35b}$$

and substituting the resulting expressions into (31a), one obtains

$$\dot{J} = \frac{\partial}{\partial Z}\left[\mathcal{D}\frac{\partial J}{\partial Z} - \mathcal{A}J\right]. \tag{36}$$

As for (23), $\mathcal{D}$ and $\mathcal{A}$ play the role of the diffusion coefficient and advection velocity, respectively. In this case too, the condition (32b), although written only for P_{c}^{zZ}, stems from a condition imposed on the overall axial stress $P^{zZ} = -p + P_{\mathrm{c}}^{zZ}$.

Consistently with (35a) and (35b), $\mathcal{D}$ and $\mathcal{A}$ can be expressed constitutively as functions of J and Z. As for the unconfined compression test, the approach based on (36) lowers by one the order of the spatial derivatives of $\mathfrak{g}$ featuring in (31a), but treats J as a free unknown of the model. Therefore, the final form of the model equations reads

$$\frac{\partial \mathfrak{g}}{\partial Z} = J, \tag{37a}$$

$$\frac{\partial p}{\partial Z} = \frac{\partial \tilde{P}_{\mathrm{c}}^{zZ}}{\partial Z}, \tag{37b}$$

$$\dot{J} = \frac{\partial}{\partial Z}\left[\mathcal{D}\frac{\partial J}{\partial Z} - \mathcal{A}J\right]. \tag{37c}$$

The set (37a)–(37c) comprises three independent scalar equations in the three unknowns $\mathfrak{g}$, J and p and is, thus, closed. The boundary conditions must be rephrased compatibly with the new formulation. In the case of a displacement-controlled confined compression test, the boundary conditions become

$$\mathfrak{g}(0,t) = 0, \tag{38a}$$

$$\left(\mathcal{D}\frac{\partial J}{\partial Z} - \mathcal{A}J\right)\Big|_{Z=0} = 0, \tag{38b}$$

$$\int_0^H J(\bar{Z},t)\mathrm{d}\bar{Z} = H - u_T[1-\exp(-t/t_u)]. \tag{38c}$$

$$p(H,t) = 0, \tag{38d}$$

which have to hold at all times $t \in [0, T]$. Equation (38b) is a homogeneous Robin condition on J.

Since (37a) and (37b) are decoupled from (37c), they can be solved *a posteriori*, once J is determined by means of (37c). In particular, it is possible to directly integrate (37a) and (37b), i.e.,

$$\mathfrak{g}(Z,t) = \int_0^Z J(\bar{Z},t)\mathrm{d}\bar{Z}\,, \tag{39a}$$

$$p(Z,t) = \tilde{P}_{\mathrm{c}}^{zZ}(J(Z,t),Z) - \tilde{P}_{\mathrm{c}}^{zZ}(J(H,t),H)\,. \tag{39b}$$

5.4 Discretisation and Results

The numerical solution to (37c) is determined by using central differences for the space derivatives, and an ordinary differential equation (ODE) solver for the time derivatives [12]. The computational domain $[0, H]$ is partitioned as $0 = Z_1 < \ldots < Z_M = H$, which determines $M - 1$ subintervals. In the procedure adopted in this work, all subintervals have the same length Δ. Moreover, for the sake of a lighter notation, the identification $P_{\mathrm{c}}^{zZ} \equiv P$ is made. At the mth grid node, with $m = 2, \ldots, (M-1)$, the spatially discretised from of (37c) is given by

$$\dot{J}_m = \frac{1}{\Delta^2}\left[\frac{k_{m+1}}{J_{m+1}}(P_{m+1} - P_m) - \frac{k_m}{J_m}(P_m - P_{m-1})\right]\,. \tag{40}$$

Note that the nodes Z_m, with $m = 2, \ldots, M-1$, belong to the interior of the computational domain. The values J_1 and J_M, which correspond to the boundary nodes, must be determined in compliance with the conditions (38b) and (38c). Furthermore, to maintain the second-order-accuracy of the discretisation scheme, a fictitious node $Z_0 < Z_1$ is introduced, so that the partial derivative of J featuring in the Robin condition (38b) can be approximated by means of the central difference $(J_2 - J_0)/(2\Delta)$ [12]. The ODEs (40) are then solved in time by using a stable ODE solver, with initial condition $J_m(0) = 1$, for all $m = 1, \ldots, M$. All numerical simulations have been performed both in Fortran and in Matlab©.

For the confined compression test, P_{c}^{zZ} is given by

$$P_{\mathrm{c}}^{zZ} = \tilde{P}_{\mathrm{c}}^{zZ}(J,Z) = \tfrac{1}{2}A(Z)\exp\left[(J^2-1)\beta\right]\frac{J^2-1}{J^{2\beta+1}}\,, \tag{41}$$

where $A = 4\,\alpha_0\,\beta = 4\,\alpha_0\,(\alpha_1 + 2\alpha_2)$ [5] is the aggregate elastic modulus (i.e., the stiffness in uni-axial deformation in the linear theory, given by the component L^{ZZZZ} of the (material) linear elasticity tensor $\mathbb{L}$), and α_0, α_1, α_2, β are the material constants in the Holmes-Mow hyperelastic potential (8).

For this numerical implementation, the undeformed permeability k_0 is obtained by extrapolating the experimental data taken from [10], and the material parameter $\alpha_0 = A/(4\beta)$ is obtained from the values of the aggregate modulus A from the experimental

reported in [11]. Both are expressed by third-order polynomials in the normalised depth Z/H, i.e.,

$$k_0(Z) = \big[-1.4485 \left(\tfrac{Z}{H}\right)^3 + 1.4813 \left(\tfrac{Z}{H}\right)^2 + 0.0193 \left(\tfrac{Z}{H}\right) + 0.1371 \big] \cdot 10^{-3} \mathrm{mm}^2 \mathrm{MPa}^{-1} \mathrm{s}^{-1}, \tag{42}$$

$$\alpha_0(Z) = \big[-1.4953 \left(\tfrac{Z}{H}\right)^3 + 3.3255 \left(\tfrac{Z}{H}\right)^2 - 2.6711 \left(\tfrac{Z}{H}\right) + 0.8471 \big] \ \mathrm{MPa}\,, \tag{43}$$

whereas all other parameters are the same as for the case of unconfined compression ($M = 4.638$, $\gamma = 0.0848$, and $\phi_{\mathrm{sR}} = 0.2$ from [5], $\alpha_1 = 0.26$ and $\alpha_2 = 0.25$, whose values are assumed, and $\beta = \alpha_1 + 2\alpha_2 = 0.76$ from [5]). In this case too, the specimen is a cylinder of initial height $H = 2$ mm and radius $R_{\mathrm{ext}} = 3$ mm. The target value and time constant of the imposed axial displacement are $u_T = 0.4$ mm (corresponding to a final 20% nominal strain) and $t_u = 10$ s.

Because of the inhomogeneous material properties, the volume ratio J is inhomogeneous through the (normalised) depth of the sample also at stationary state; in particular, the much lower stiffness $\alpha_0 = A/(4\beta)$ in the superficial zone (close to $Z = 1$) makes the volumetric compression extreme for the considered overall deformation, with values of $J \simeq 0.30$ (Fig. 3). Since the pressure p must be zero on the upper boundary, the absolute value of the axial component P_{c}^{zZ} of the constitutive part of the first Piola-Kirchhoff stress (normalised to the value $\alpha_0(0)$ that the material parameter α_0 takes at $Z = 0$) is largest at the upper boundary and equals the absolute value of the total (normalised) stress P^{zZ}; at the end of the test, stationary state is practically achieved, as p is zero and consequently P_{c}^{zZ} is uniform throughout the tissue depth (Fig. 4).

6 Discussion

In this work, following the lines of Armstrong et al. [4], who studied unconfined compression of isotropic homogenous cartilage under small deformations, and of Holmes and Mow [5], who studied confined compression of homogenous isotropic cartilage under large deformations, we addressed the unconfined case in the large-deformation setting, and the confined case by removing the hypothesis of homogeneity, thereby allowing some of the material properties to vary along the axis of compression. In both the cases of unconfined and confined compression, we reduced the problem to a diffusion-advection equation in J, which was regarded as the relevant kinematical variable. A result similar to the diffusion-advection equation (36) of the confined case was obtained in [12]. There are, however, two major differences between the two approaches. Firstly, the model analysed in [12] was homogeneous and, consequently, could not obtain the advection "velocity" $\mathcal{A}$. This "velocity", indeed, arises because of the inhomogeneity of the constitutive law of the axial stress. Secondly, in [12], tissue remodelling (an anelastic process) was considered, and the hydraulic and mechanical behaviour of the specimen was studied in the elastic range subsequent remodelling.

Although more precise descriptions of articular cartilage have been given [9,15,16], where the inhomogeneity and anisotropy of the tissue induced by the presence of the

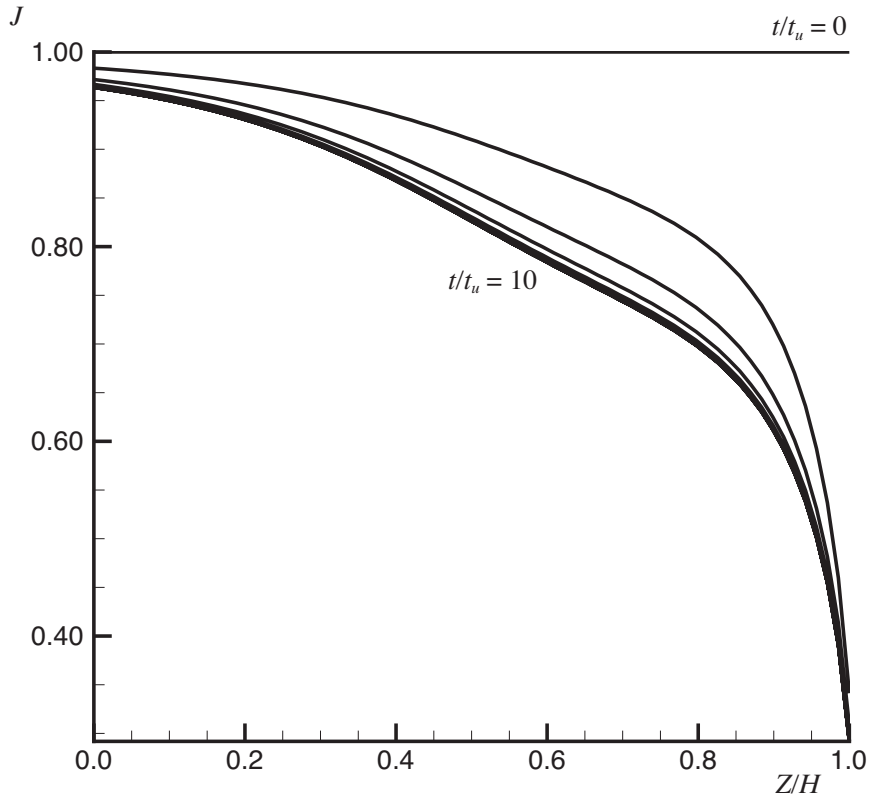

Figure 3: Volume ratio J vs the normalised axial coordinate Z/H. The curves are plotted for values of the normalised time $t/t_u = 0, 1, ..., 10$.

collagen fibres have been considered, and more general constitutive models can be conceived to include effects such as growth and remodelling (cf., e.g., [17, 18]), the mathematical formulation presented in this work is based on the non-linear biphasic (solid-fluid) model. Since we are working with an established theory, and the only "arbitrary" choice is that on the constitutive equations, we believe that, by fitting parameters, the vast majority of experimental confined or unconfined tests could validate our numerical simulations. However, it is clear that homogeneous and isotropic cartilage does not exist and therefore the unconfined case would certainly be a rather artificial fitting of material parameters. Moreover, to the best of our knowledge, there is *no* confined compression test in which both the elastic properties and the permeability have been evaluated. Indeed, the permeability measurements performed by Maroudas and Bullough [10] do not involve any compression test and, conversely, the compression tests performed by Schinagl et al. [11] do not involve any permeability measurement. Specifically, the inhomogeneous permeability measurements performed by Maroudas and Bullough [10] are the only ones we are aware of. Therefore, we cannot infer that our results can have direct experimental validation. As far as a comparison with other computational models

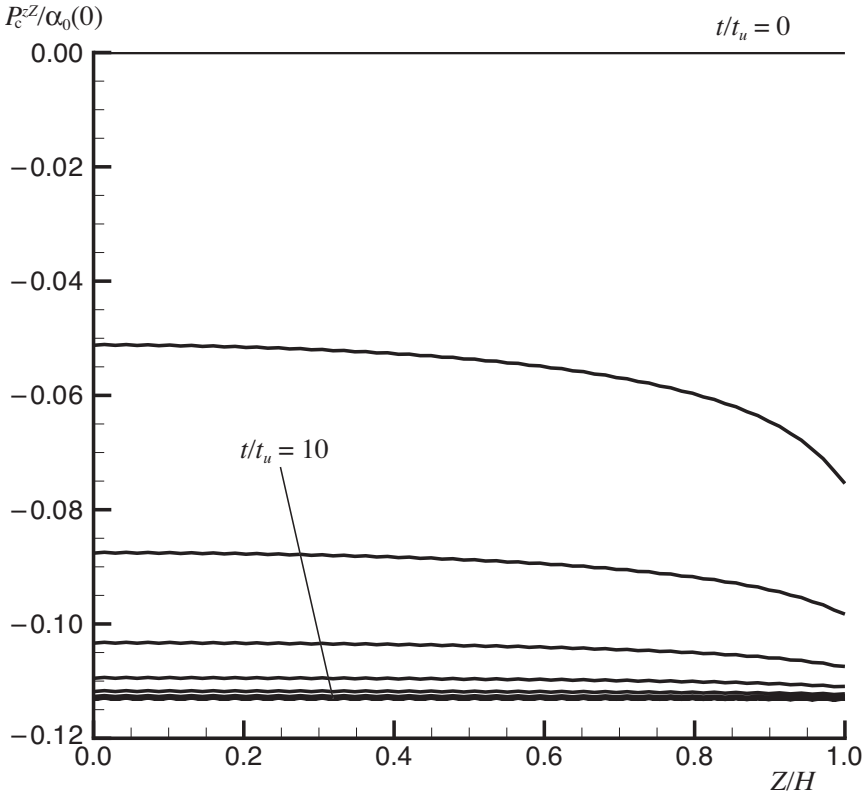

Figure 4: Axial component P_c^{zZ} of the constitutive part of the first Piola-Kirchhoff stress tensor of the solid phase, normalised to the value $\alpha_0(0)$ of the material parameter α_0 at $Z = 0$, vs the normalised axial coordinate Z/H. The curves are plotted for values of the normalised time $t/t_u = 0, 1, ..., 10$.

is concerned, the theoretical derivation of our model has been obtained by simplifying the theory of biphasic mixtures comprising an inviscid fluid and a hyperelastic solid material under the assumption that both phases are incompressible. In this respect, our theoretical results are expected to be consistent with those obtained by the inhomogeneous and anisotropic theory, if the appropriate model reductions are made.

One of the limitations of the method presented here is the isotropy of the material properties. Indeed, mostly due the presence of the collagen fibres, articular cartilage exhibits anisotropic behaviour in both its elastic properties (see, e.g., [9, 16, 19]) and permeability (see, e.g., [8, 9, 15, 16, 20]). However, the anisotropy of the tissue was not taken into account here, since the purpose of this work is to show how much information about the mechanical and hydraulic behaviour of the tissue can be extracted also from much simpler models, which do not require elaborated numerical procedures such as the Finite Element Method. Note that neither the fluid inside the cells, nor the intrafibrillar fluid [21, 22] are explicitly accounted for in the presented model. Con-

sidering these fluids, along with the ions dissolved in them, and their interaction with all the other constituents of the tissue would call for a full electro-chemo-mechanical approach, whose solution would require the employment of sophisticated numerical procedures, especially when large deformations occur. Such a detailed level of modelling is out of the scopes of this paper. The proposed approach is valid also in more complex cases, as long as the further complication is in the non-linearity of the constitutive laws, but ceases to be applicable when the added complication breaks one or more symmetries of the problem. In this case, Finite Element methods often become indispensable.

In our opinion, the advantage of using Finite Differences against Finite Element methods for the problems at hand lies in the fact that the problem reduction shown in the manuscript makes it sufficient to employ one-dimensional grids for solving the model equations in a sufficiently stable, efficient and accurate way, while keeping the computational costs at an acceptable level. This is due to the fact that each of the considered problems is reduced to a set of partial differential equations in which the space dependence appears solely in the partial derivatives with respect to the radial coordinate (in the unconfined compression) or to the axial coordinate (in the confined compression).

The importance of this work is, in fact, in the possibility of testing a given material behaviour (or, more precisely, the isotropic version of a material behaviour) in a non-trivial, biphasic, large deformation setting. This means that the result of the Finite Element implementation of a user-defined material can be tested against the proposed method, which gives full control on all physical quantities, since it is based directly on the governing differential equations.

Acknowledgements

Alberta Innovates - Technology Futures (Canada) [SF], Alberta Innovates - Health Solutions (Canada) [SF], the Natural Sciences and Engineering Research Council of Canada [SF], the Start-up Packages and PhD Program Project, co-funded by Regione Lombardia (Italy) [CG], and the Progetto Giovani GNFM 2014 funded by the Italian National Group of Mathematical Physics [CG].

References

[1] Torzilli, P. A., and Mow, V. C. "On the fundamental fluid transport mechanisms through normal and pathological articular cartilage during function - I - the formulation". *J. Biomech.,* **9**: 541–552, 1976.

[2] Torzilli, P. A., and Mow, V. C. "On the fundamental fluid transport mechanisms through normal and pathological articular cartilage during function - II - the analysis, solution and conclusions". *J. Biomech.,* **9**: 587–606, 1976.

[3] Mow, V. C., Kuei, S. C., Lai, W. M., and Armstrong, C. "Biphasic creep and stress relaxation of articular cartilage in compression: Theory and experiments". *J. Biomech. Eng.,* **102**: 73–84, 1980.

[4] Armstrong, C. G., Lai, W. M., and Mow, V. C. "An analysis to unconfined compression of articular cartilage". *J. Biomech.,* **106**: 165–173, 1984.

[5] Holmes, M. H., and Mow, V. C. "The nonlinear characteristics of soft gels and hydrated connective tissues in ultrafiltration". *J. Biomech.,* **23**: 1145–1156, 1990.

[6] Federico, S., Grillo, A., Giaquinta, G., and Herzog, W. "A semi-analytical solution for the confined compression of hydrated soft tissue". *Meccanica,* **44**: 197–205, 2009.

[7] Grillo, A., Federico, S., Wittum, G., Imatani, S., Giaquinta, G., and Mićunović, M. V. "Evolution of a fibre-reinforced growing mixture". *Nuovo Cimento C,* **32C**: 97–119, 2009.

[8] Federico, S., and Grillo, A. "Elasticity and permeability of porous fibre-reinforced materials under large deformations". *Mech. Mat.,* **44**: 58–71, 2012.

[9] Tomic, A., Grillo, A., and Federico, S. "Poroelastic materials reinforced by statistically oriented fibres - numerical implementation and application to articular cartilage". *IMA J. Appl. Math.,* **79**: 1027–1059, 2014.

[10] Maroudas, A., and Bullough, P. "Permeability of articular cartilage". *Nature,* **219**: 1260–1261, 1968.

[11] Schinagl, R. M., Gurskis, D., Chen, A. C., and Sah, R. L. "Depth-dependent confined compression modulus of full-thickness bovine articular cartilage". *J. Orthop. Res.,* **15**: 499–506, 1997.

[12] Grillo, A., Giverso, C., Favino, M., Krause, R., Lampe, M., and Wittum, G. "Mass transport in porous media with variable mass". In *Numerical Analysis of Heat and Mass Transfer in Porous Media — Advanced and Structured Materials*, J. M. P. Q. Delgado, A. G. B. de Lima, and M. V. d. Silva, eds. Springer-Verlag, Berlin Heidelberg, 27–61, 2012.

[13] Madeo, A., dell'Isola, F., and Darve, F. "A continuum model for deformable, second gradient porous media partially saturated with compressible fluids". *J. Mech. Phys. Solids,* **61**: 2196–2211, 2013.

[14] Ateshian, G. A., and Weiss, J. A. "Anisotropic hydraulic permeability under finite deformation". *J. Biomech. Eng.,* **132**: 111004, 2010.

[15] Federico, S., and Herzog, W. "On the anisotropy and inhomogeneity of permeability in articular cartilage". *Biomech. Model. Mechanobiol.,* **7**: 367–378, 2008.

[16] Pierce, D. M., Ricken, T., and Holzapfel, G. A. "A hyperelastic biphasic fibre-reinforced model of articular cartilage considering distributed collagen fibre orientations: continuum basis, computational aspects and applications". *Comput. Meth. Biomech. Biomed. Eng.,* **16**: 1344–1361, 2013.

[17] Lekszycki, T., and dell'Isola, F. "A mixture model with evolving mass densities for describing synthesis and resorption phenomena in bones reconstructed with bio-resorbable materials". *Z. Angew. Math. Mech.,* **92**: 426–444, 2012.

[18] Andreaus, U., Giorgio, I., and Madeo, A. "Modeling of the interaction between bone tissue and resorbable biomaterial as linear elastic materials with voids". *Z. Angew. Math. Phys.*, 2015.

[19] Wilson, W., Huyghe, J. M., and van Donkelaar, C. C. "Depth-dependent compressive equilibrium properties of articular cartilage explained by its composition". *Biomech. Model. Mechanobiol.,* **6**: 43–53, 2007.

[20] Federico, S., and Herzog, W. "On the permeability of fibre-reinforced porous materials". *Int. J. Solids Struct.,* **45**: 2160–2172, 2008.

[21] Loret, B., and Simoes, F. M. F. "Articular cartilage with intra- and extrafibrillar waters: a chemo-mechanical model". *Mech. Mat.,* **36**: 515–541, 2004.

[22] Loret, B., and Simoes, F. M. F. "A framework for deformation, generalized diffusion and growth in multi-species multi-phase biological tissues". *Eur. J. Mech. A/Solids,* **24**: 757–781, 2005.

MOX Technical Reports, last issues

Dipartimento di Matematica
Politecnico di Milano, Via Bonardi 9 - 20133 Milano (Italy)

49/2015 Ghiglietti, A.; Ieva, F.; Paganoni, A.M.
Statistical inference for stochastic processes: two sample hypothesis tests

47/2015 Colombo, M. C.; Giverso, C.; Faggiano, E.; Boffano,C.; Acerbi, F.; Ciarletta, P.
Towards the personalized treatment of glioblastoma: integrating patient-specific clinical data in a continuous mechanical model

48/2015 Ambrosi, D.; Pettinati, V.; Ciarletta, P.
Active stress as a local regulator of global size in morphogenesis

45/2015 Lange, M.; Palamara, S.; Lassila, T.; Vergara, C.; Quarteroni, A.; Frangi, A.F.
Improved hybrid/GPU algorithm for solving cardiac electrophysiology problems on Purkinje networks

46/2015 Giverso, C.; Verani, M.; Ciarletta P.
Emerging morphologies in round bacterial colonies: comparing volumetric versus chemotactic expansion

44/2015 Antonietti, P.F.; Houston, P.; Smears, I.
A note on optimal spectral bounds for nonoverlapping domain decomposition preconditioners for hp-Version Discontinuous Galerkin methods

43/2015 Deparis, S.; Forti, D.; Gervasio, P.; Quarteroni, A.
INTERNODES: an accurate interpolation-based method for coupling the Galerkin solutions of PDEs on subdomains featuring non-conforming interfaces

42/2015 Brugiapaglia, S.; Nobile, F.; Micheletti, S.; Perotto, S.
A theoretical study of COmpRessed SolvING for advection-diffusion-reaction problems

41/2015 Quarteroni, A.; Veneziani, A.; Vergara, C.
Geometric multiscale modeling of the cardiovascular system, between theory and practice

40/2015 Patelli, A.S.; Dedè, L.; Lassila, T.; Bartezzaghi, A.; Quarteroni, A.
Isogeometric approximation of cardiac electrophysiology models on surfaces: an accuracy study with application to the human left atrium